Novel MIMO Technique for Wireless Terabits Systems in sub-THz Band

Majed Saad, Nour Al Akkad, Hussein Hijazi, Ali Chamas Al Ghouwayel, Faouzi Bader, Jacques Palicot

Novel MIMO Technique for Wireless Terabits Systems in sub-THz Band

Majed Saad, Nour Al Akkad, Hussein Hijazi, Ali Chamas Al Ghouwayel, Faouzi Bader and Jacques Palicot.

***Abstract*—In this paper, a generalized MIMO Spatial Multiplexing (SMX) system with a new Index Modulation (IM) domain called filter IM domain is proposed. This filter domain generalizes the time and frequency IM domains. In particular, a Filter Shape IM (FSIM) is used to virtually transmit a part of the information bitstream by indexing the filter shape varying at the symbol rate. This scheme permits to achieve high Spectral Efficiency (SE) since it uses all the available time, frequency, and spatial resources. The proposed transceiver can be easily reconfigured to operate as a conventional MIMO SMX transceiver. Compared to the existing systems, the proposed system achieves the highest SE gain with the help of IM and MIMO multiplexing gain. The theoretical lower bound is derived to characterize the SMX FSIM system performance. The results reveal that SMX FSIM with 2 filter shapes only outperforms by 3.5 dB up to more than 12 dB the equivalent SMX QAM system at the same SE. Furthermore, a complete analysis in the sub-THz indoor environment with RF impairments is provided for the proposed system, SMX QAM, and Generalized Spatial Modulation. Finally, the results show that SMX FSIM with a linear receiver has better performance and robustness to phase noise, lower transceiver cost, higher SE/energy efficiency gain, and lower power consumption.**

***Index Terms*—Index Modulation (IM), Filter Index Modulation, Filter Domain (FD), Filter Shape Index Modulation (FSIM), pulse shaping filter, joint maximum likelihood detector, matched filter detector, spectral efficiency, energy efficiency, SISO.**

I. Introduction

The wireless data traffic is expected to increase by more than 10000-fold by the year 2030 [1]. Correspondingly, the data rates required are increasing continuously towards Terabits per second (Tbps). To accommodate this enormous expected boost in traffic demand, either shrinking cell sizes, dramatically increasing spectral efficiency, acquiring extra bandwidth, or having a mixture of all three, will improve the throughput per square meter in a wireless network that 5G cannot cope with [1]. The millimeter-wave and sub-TeraHertz (THz) bands can provide a huge bandwidth, but more challenges and limitations appear in the path towards beyond 5G systems. In the context of BRAVE project [2], [3], we target to define new wireless technologies for sub-THz bands that can achieve ultra-high data rates in the order of Tbps. The exploitation of the sub-THz bands mainly between 90 and 200 GHz with a 58.1 GHz total available bandwidth can help to reach Beyond 5G data rate requirements with current electronics technology.

Multiple-Input-Multiple-Output (MIMO) technology and mainly Spatial Multiplexing (SMX) is a key enabler for high data rate applications that was combined with high order QAM in recent standards for high data rate. MIMO systems caught significant attention because of their superiority in exploiting spatial resources, improving system capacity, and increasing the Spectral Efficiency (SE). However, increasing the order of QAM modulation in the sub-THz band is limited by the RF impairments and limitations (e.g., Phase Noise (PN), low output power, hardware non-linearity,...) [4]. Thus, better exploitation of MIMO technology is required to enable a low-power ultra-high data rate system in sub-THz bands while surviving with the Radio Frequency (RF) impairments and sub-THz limitations.

Index Modulation (IM) has attracted considerable attention in the last decades due to significant enhancement in the system Energy Efficiency (EE) and/or spectral efficiency, which is beneficial for low-power and/or ultra-high data rates applications. IM's general concept is to encapsulate additional information bits (Virtual Bits (VB)) in an index of an element that can be detected at the receiver side to recover these bits. Basically, the three main IM domains are: spatial, time, and frequency domains where the indexation is applied by activating one or more antenna(s) [5]–[9], time slot(s) [10], [11], and subcarrier(s)/frequency band(s) [12]–[14] respectively.

The spatial IM domain can provide high SE gain, mainly when it also exploits the multiplexing gain. For instance, Generalized Spatial Modulation (GSM) conveys the information bits in the index of the activated Transmit Antenna Combination (TAC) and in the N_a simultaneously transmitted symbols [7]. Note that GSM generalizes several existing schemes such as Space Shift Keying (SSK) [6] (and its generalized version GSSK [15]) with single (multiple) active Transmit Antenna TA(s) without any Amplitude Phase Modulation (APM) symbol, also Spatial Modulation (SM) [5] with APM symbol and single active TA. It is worth mentioning that GSM system with power-efficient modulation (e.g. QPSK) is a promising candidate for the sub-THz system even with a medium PN level when the optimal detection is considered [4], [16]. However, it has some performance degradation with highly correlated channels like those in sub-THz bands, but it can be reduced by an efficient legitimate TAC set selection and spatial bit-mapping [17].

In the Single-Input-Single-Output (SISO) context, the fre-

M. Saad, J. Palicot are with SCEE-Signal, Communication & Embedded Electronics research group, CentraleSupélec\IETR-Campus of Rennes, Cesson-Sévigné, 35510 Brittany-France e-mail: majed.saad@ieee.org, jacques.palicot@supelec.fr.

N. Al Akkad and H. Hijazi are with CCE department, Lebanese International University, Lebanon email: 31530088@students.liu.edu.lb, hussein.hijazi@liu.edu.lb.

A. Chamas Al Ghouwayel is with the School of Engineering EFREI, 94800 Villejuif-Paris, France email: ali.ghouwayel@efrei.fr

Faouzi Bader is with Institut Supérieur d'Electronique de Paris, 75006 Paris, France email: carlos.bader@isep.fr.

quency and time IM domains suffer from low SE gain and even loss with high order modulation scheme due to discarding some time/frequency resources. For clarification, the Orthogonal-Frequency-Division-Multiplexing OFDM-IM technique [12], [13] in frequency IM domain conveys the VB in the combination of activated sub-carries while providing better performance at low data rates and lower complexity at the price of SE loss with high order modulation. In addition, some extensions in this domain try to recover some of the SE loss by using a variable number of activated subcarriers and/or separate indexation for the in-phase and quadrature components [14]. However, all these schemes suffer from high Peak-to-Average Power Ratio (PAPR) and SE loss with high modulation order compared to conventional systems with APM (e.g., QAM, PSK). Similarly, Single-Carrier-IM (SC-IM) in time IM domain that conveys the VB through the combination of activated time slots [10] has the same drawback in SE but with a lower PAPR and substantial EE gain. For better compensation of SE loss, non-orthogonal schemes are explored in time and frequency IM domains (SC Faster-Than-Nyquist IM SC-FTN-IM [11], and Spectral Efficient FDM-IM (SEFDM-IM) [18] respectively). These schemes are similar to their orthogonal version but in a compressed form in time or frequency dimension that leads to inherited interference.

Recently, a novel domain for IM named "Filter domain" is proposed in [19]. This new dimension generalizes many existing modulations and SISO-IM domains (e.g., time and frequency IM domains described previously). The frequency IM domain can be seen as a special case of the filter IM domain because the activation/deactivation of a frequency band or a subcarrier is just an application of a bandpass/zero filter. Similarly, the time IM domain counterpart and many other existing modulation schemes can also be considered as a special case of the filter IM domain, as discussed in [19]. The filter IM domain also allows us to achieve the highest SE gain in SISO since it can be configured to fully use all the available time and frequency resources. A Filter Shape IM (FSIM) was also proposed in [19], where the information bits are emitted through APM symbol and index of a transmit filter that can be changed at the symbol rate. At the transmitter side, a filter bank with N different pulse shaping filters is used to explore the indexation gain that leads to $\log_2 N$ as SE enhancement in SISO-FSIM.

In this paper, a generalized SMX system is proposed motivated by the different advantages of FSIM scheme and its generalizations for various existing IM schemes. Thus, this system includes different existing schemes as special cases (e.g., SMX with conventional APM, MIMO-OFDM-IM [20], and SMX with any time/frequency IM), since filter IM domain can be configured to change the emitted symbol [19]. The transmission of different FSIM symbols from the TAs allows achieving a higher SE and EE gain. In other words, any small SE enhancement by FSIM in SISO has a tremendous impact when it is extended to MIMO system, where the overall SE gain by SMX FSIM compared to SMX QAM is $N_t \log_2 N$ for $N_t \leq N_r$. In addition, a simple receiver for SMX-FSIM is presented in this paper, where a sample level equalization is performed, and followed by a parallel Matched Filter (MF) based detector. Moreover, the theoretical system performance is derived and validated by Monte Carlo simulations and then compared with other equivalent systems.

The main contributions are summarized as follows:

1) A generalized MIMO SMX system is proposed by incorporating FSIM scheme to achieve high SE and EE gain. The proposed SMX-FSIM system conveys information bits in the signal and filter IM domains. The VBs are encapsulated by the different filter shapes indices that are used for pulse shaping of the N_t simultaneously transmitted APM symbols. Note that the transmit spatial IM (e.g., GSM system) conveys all the VBs by a single index (index of activated TAC), and its misdetection leads to bit errors in most of the VBs and also in the real bits of all transmitted APM symbols (i.e., N_a APM symbols in GSM will be most probably mis-detected when an error occurs in the TAC index detection). However, the decentralization of VBs encapsulation in SMX-FSIM avoids the highlighted single point of failure in GSM system.
2) A simple receiver for SMX-FSIM is presented, which is based on Zero-Forcing (ZF) sample level equalizer followed by a parallel MF-based detector. The proposed parallel detection for SMX-FSIM provides good performance with prominent complexity reduction compared to the joint Maximum Likelihood (ML)-based detector.
3) The analytical performance of SMX-FSIM using ZF equalizer is derived and validated by Monte Carlos simulations. Then, they are compared to those of the conventional SMX QAM system of the same SE. The results show an important SE and EE gain can be achieved even with a low number of filter shapes.
4) The performance of the proposed SMX FSIM scheme is evaluated under sub-THz channels with RF impairments, then compared to the existing ultra-high data rate candidates (GSM and conventional SMX QAM [4]).
5) These sub-THz candidates are compared and analyzed from different perspectives (performance, robustness to PN, SE/EE, cost, PAPR, and power consumption). The results reveal that the spectrally efficient SMX-FSIM with power-efficient APM is the best promising candidate for such systems in sub-THz bands because it has better performance and robustness to PN, higher SE and EE gain, lower power consumption and cost, as well as it avoids the RF switching problem that appears with transmitter spatial IM (e.g., GSM).

This paper is organized as follows. In Section II, the SMX-FSIM system model is described, whereas the theoretical performance derivations and analysis of the lower bound is presented in section III. Section IV firstly presents the comparison of the proposed system with the widely used existing equivalent MIMO systems based on numerical and theoretical results. Afterward, the system evaluation in the sub-THz environment is also provided in Section IV, along with a complete analysis of the considered candidates. Finally, Section V concludes the paper.

The notations adopted in this paper are as follows. Bold

lower (upper) case is used for vectors (matrices). The character $*$ denotes the convolution. $(.)^H$, $(.)^T$ and $(.)^{-1}$ are used to denote respectively the Hermitian transpose, the transpose and the inverse of a matrix. $\langle x, y\rangle$ stands for the dot-product. $\mathcal{CN}(\mu, \sigma^2)$ denotes the complex normal distribution of a random variable having mean μ and variance σ^2. $\lfloor x \rfloor$ ($\lceil x \rceil$) denotes the floor (ceil) function that means the largest (smallest) integer less (greater) than or equal to x. $\|.\|$ stands for the Frobenius norm. The probability of an event is denoted by $P(.)$ and the Probability Density Function (PDF) is denoted by $p(.)$. $\mathbb{E}[.]$ denotes the expectation. C_n^k (n choose k) denotes the binomial coefficient.

II. System Model: MIMO Spatial Multiplexing with FSIM

In the design of the novel FSIM based MIMO transceiver and its analysis, we considered most of the sub-THz band's peculiarities. In particular, the following points technological limitations, RF impairments, and sub-THz channel characteristics are considered in the waveform and system design phase:

- Low output transmit output power with limited achievable SNR [4]. Thus, the new sub-THz waveform should be energy efficient to maintain good performance.
- Important RF impairments such as carrier frequency offset (CFO) and phase noise of the oscillator that increase at higher frequencies [21]. The CFO can be estimated and canceled, but the PN's dominant term in a wide sub-THz band that cannot be completely compensated is the random Gaussian process. This random term of the PN has the highest impact on performance degradation [22]. Thus, a waveform robust to PN is required to maintain a good performance with the residual PN.
- A low data converters resolution (quantization levels) is preferred to avoid the high cost and power of the ultra-high sampling rate data converters (ADC/DAC) with high resolution.
- The efficient wireless link in sub-THz bands is composed of the Line-of-Sight dominant path in most cases with/without few survival non-line-of-sight paths.

Therefore, in our approach to design the proposed novel MIMO transceiver, we insist on using a power-efficient single carrier modulation with low order modulation to provide better robustness for sub-THz bands and survive with these limitations. However, to reach ultra-high data rates in the order of Terabits per second, a spectral efficient IM technique is required even with the large available bandwidth, and thus we exploited our novel Index Modulation domain "Filter IM domain". The proposed system will enhance the SE by exploiting all available time, frequency, and spatial resources in contrast to most IM domains. Moreover, the proposed SMX-FSIM transceiver will also enhance the EE because the VBs, in general, can be detected at lower SNR, as it will be confirmed in Section IV.

A. SMX FSIM Transmitter

Consider a $N_t \times N_r$ MIMO-SMX system ($N_t \leq N_r$), where N_t and N_r are the number of transmit and receive antennas respectively. In this paper, FSIM scheme that conveys information bits by the index of the different filter shapes and the APM symbols is considered to achieve high SE and EE gain. Note that this system SMX-FSIM in the filter IM domain allows to use all available resources in contrast to other IM domains (time, frequency, antennas, etc.).

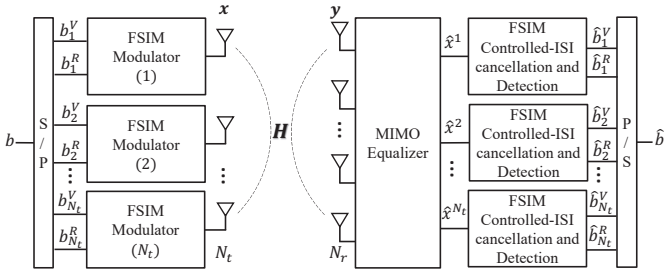

Fig. 1. System model of $N_t \times N_r$ SMX-FSIM transceiver.

The input bitstream b is divided into N_t sub-streams $b_1, b_2, ..b_{N_t}$, as shown in Figure 1, and passed through its corresponding FSIM modulator.

Each sub-stream b_j contains the real and virtual information bits denoted by b_j^R and b_j^V respectively. The former is mapped using the M-ary APM (e.g., QAM, PSK), while the latter is translated to an index i^j, which represents the index of the selected filter f_{i^j} at the j^{th} TA. Then, the APM symbol c^j is pulse shaped, as depicted in Fig. 2, using the filter $f_{i^j}[m]$ of length L samples with m is the sample index from 0 to $L-1$. Note that the filter is truncated in the time domain to η APM symbols, and it is sampled at a rate of λ samples per symbol, which yields $L = \eta.\lambda+1$. Then, the FSIM modulators' outputs are transmitted simultaneously from the N_t TAs.

The filter bank for each FSIM modulator shown in Fig. 2 includes N different filter shapes where N is a power of 2. Without loss of generality, we consider that SMX-FSIM uses the same filter bank and APM for all TAs. Subsequently, the total number of bits per SMX-FSIM symbol $\text{SE}_{\text{SMX-FSIM}}$ can be expressed as:

$$\begin{aligned}\mathcal{L}_{\text{SMX-FSIM}} &= N_t(\log_2 N + \log_2 M) \\ &= N_t \log_2 N + \mathcal{L}_{\text{SMX-QAM}},\end{aligned} \tag{1}$$

where $\mathcal{L}_{\text{SMX-QAM}} = N_t \log_2 M$ is the number of transmitted bits of a conventional MIMO-SMX system with N_t TAs and M-ary APM. It is clear that the SE gain increases linearly with the number of TAs, and it is $N_t \log_2 N$ higher than that of the conventional MIMO-SMX system with the same M-ary APM.

The output of the filter bank $s_n^j[m]$ for the n^{th} APM symbol c_n^j at the j^{th} TA is:

$$s_n^j[m] = \left(f_{i_n^j} * {c_n^j}'\right)[m] = c_n^j f_{i_n^j}[m], \tag{2}$$

where ${c_n^j}'$ is the up sampled copy of c_n^j by a factor L.

Then, the signals $s_n^j[m]$ are passed through the Overlap and Add (OLA) block as shown in Fig. 2 to generate the emitted

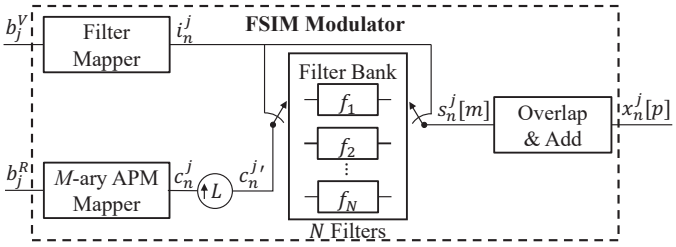

Fig. 2. System model of FSIM Modulator with M-ary APM mapping and a filter bank of N filters.

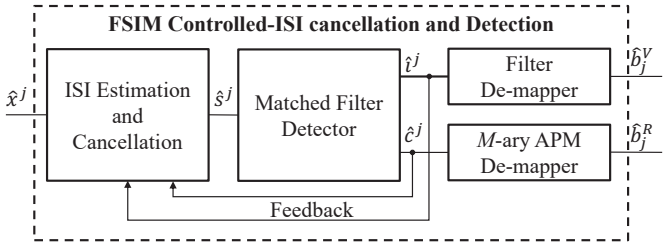

Fig. 3. System model of FSIM demodulator with the controlled-ISI cancellation and detection.

signal $x_n^j[p]$ as follows:

$$x_n^j[p] = \sum_{n'=n-\lceil \eta/2 \rceil}^{n+\lfloor \eta/2 \rfloor} s^j{}_{n'}[p-(n'-n)\lambda], \tag{3}$$

where the index $p = p_{\text{center}} - \lceil \lambda/2 \rceil + 1, ..., p_{\text{center}} + \lfloor \lambda/2 \rfloor$ and the index of the middle desired sample is $p_{\text{center}} = \frac{L-1}{2}$ [19]. Note the used filters introduce Inter-Symbol Interference (ISI) since Nyquist condition for zero ISI is relaxed in FSIM scheme to achieve higher SE by indexing distinguishable filter shapes.

B. SMX-FSIM Receiver

1) Equalization: At the receiver, the received signal in time domain $\mathbf{y}$ can be expressed as:

$$\mathbf{y} = \mathbf{H}\mathbf{x} + \mathbf{v}, \tag{4}$$

where $\mathbf{H} = [\mathbf{h}_1, ..., \mathbf{h}_{N_t}]$ is the $N_r \times N_t$ MIMO channel matrix with $\mathbf{h}_i$ is the column vector of N_r elements, $\mathbf{x} = [x_1, \ldots, x_{N_t}]^T$ is the transmitted vector that contains N_t different FSIM symbols, $\mathbf{v}$ is $N_r \times 1$ channel noise vector and its v_r elements are complex Gaussian variables, Identically Independent Distributed (i.i.d.), with zero-mean and variance σ^2, i.e, $\mathcal{CN}(0, \sigma^2)$ for $r = 1, \ldots, N_r$.

The received signal suffers from Inter-Antenna Interference (IAI) and inter-symbol interference due to the MIMO transmission and the used non-Nyquist filters in FSIM scheme respectively. In other words, the former represents the interference from simultaneously transmitted symbols from other antennas, while the latter is the interference contribution from the previous and the future symbols emitted from the same antenna (within a filter period). When the receiver intends to detect the j^{th} FSIM symbol transmitted from the j^{th} TA, the received signal can be rewritten as follows to highlight the IAI components :

$$\mathbf{y} = \mathbf{h}_j x^j + \sum_{l=1, l\neq j}^{N_t} \mathbf{h}_l x^l + \mathbf{v}. \tag{5}$$

In addition to IAI, the symbols suffer from ISI due to filters used at the transmitter that do not satisfy Nyquist ISI criterion. At the first stage in receiver side, the received signal is passed through an equalizer to eliminate the effect of the channel $\mathbf{H}$. Note that ZF or Minimum Mean-Square Error (MMSE) equalizers can be used, or any other equalizer that conserves the FSIM filter contribution. Here the equalization is performed at sample level before matched filter and down-sampling and not at symbol level as usual, since the pulse shaping filter used at the transmitter is still unknown at this stage. In general, the THz channel matrix can be low-rank due to strong spatial sparsity. In such case equalizers like MMSE (at low and moderate SNR), OSIC or QR should be applied. But in the adopted scenario of isotropic antennas and indoor propagation where the channel is generated from a ray-based deterministic channel model [23], most of channel matrix realizations are not low rank. Thus in the following, the linear ZF equalizer is adopted to eliminate channel effect on all received samples and allow the detection of the transmitted FSIM symbol (APM symbol and index of the used filter). Then the output of the equalizer can be written as follows:

$$\hat{\mathbf{x}} = \mathbf{W}\mathbf{y} = \mathbf{x} + \mathbf{W}\mathbf{v}, \tag{6}$$

where $\hat{\mathbf{x}}$ is the vector of equalized samples and $\mathbf{W} = [\mathbf{w}_1^T, \mathbf{w}_2^T, \ldots, \mathbf{w}_{N_t}^T]^T$ is the ZF weight matrix expressed as:

$$\mathbf{W} = (\mathbf{H}^H\mathbf{H})^{-1}\mathbf{H}^H, \tag{7}$$

and $\mathbf{w}_j$ is the j^{th} row of $\mathbf{W}$.

Afterward, in order to have an effective detection of the transmitted FSIM symbol (filter index and APM symbol), the estimation and cancellation of the controlled-ISI from the used non-Nyquist filters is performed in parallel as shown in Fig. 1 on the equalized stream of samples $\hat{x}^j$ similar to the simplified SISO FSIM receiver depicted in Fig. 3.

Hence, the samples stream $\hat{x}^j$ corresponding to the j^{th} TA is passed to the ISI Estimation and Cancellation block [19], that intends to remove the ISI generated from the used filters that do not satisfy Nyquist zero-ISI criterion. The output of the ISI Cancellation block can be expressed as follows:

$$\hat{s}_n^j[m] = c_n^j f_{i_n^j}[m] + ISI_{resid}^j[m] + \mathbf{w}_j\mathbf{v}[m], \tag{8}$$

where the $ISI_{\text{resid}}^j[m]$ represents the residual ISI that might still persist due to the non-perfect ISI cancellation.

Then, for each $j = 1, \ldots, N_t$, the ISI cancellation output signal $\hat{s}_n^j[m]$ is passed through a MF-based detector to estimate the APM symbol and the index of the selected filter at the j^{th} TA.

2) Detection: In the following, the detection of the APM symbol and filter index is considered for one TA, since all TAs perform in parallel a similar detection. Each MF-based detector contains a bank of N matched filters g_k where $g_k(t) = f_k(T_f - t)$ with $0 \leq t \leq T_f$, $T_f = L.T_s$ and T_s is the

sampling period [19]. The output of these filters r_k^j sampled at the instant T_f can be expressed as follows:

$$r_k^j = \int_0^{T_f} \hat{s}^j(\tau) f_k(\tau) d\tau, \quad k = 1, 2, ..., N. \tag{9}$$

Then, the selected filter at the transmitter side on the j^{th} TA can be recovered by taking the maximum energy of the sampled MF outputs r_k^j as follows:

$$\hat{i}^j = \arg\max_k \|r_k^j\|^2. \tag{10}$$

After estimating the index of the filter being used at the j^{th} TA, the APM symbol detection is performed on $r_{\hat{i}^j}$. Afterwards, the detected symbols $\hat{c}^j$ and filter index $\hat{i}^j$ are passed to their corresponding demappers to recover the sub-streams $\hat{b}_j^R$ and $\hat{b}_j^V$ respectively. The above mentioned steps are processed in parallel for the N_t transmitted FSIM symbols, and finally the parallel to serial recovers the bitstream $\hat{b}$ as depicted in Fig. 1.

III. Theoretical Performance

In this section, the analytical lower bound in terms of Symbol Error Rate (SER) for the proposed system SMX-FSIM is derived, where we consider that the ZF equalizer and the parallel MF-based detector are used. The system performance of SMX-FSIM depends on the APM symbols and filter index detection. In addition, the lower bound theoretical SER and BER are deduced under the assumption of perfect ISI cancellation ($i.e.\ ISI_{resid} = 0$), and near-orthogonal filter shapes that can be achieved when the filter bank is well designed.

The output of the matched filter bank at j^{th} TA sampled at $t = T_f$ given by r_k^j in (9) can be rewritten as:

$$\begin{aligned} r_k^j &= \langle \mathbf{f}_k, \mathbf{f}_{i_n^j} \rangle . c_n^j + \langle \mathbf{f}_k, \mathbf{w}_j \mathbf{v}_n \rangle \\ &= \begin{cases} c_n^j + \langle \mathbf{f}_k, \mathbf{w}_j \mathbf{v}_n \rangle & \text{for } k = i_n^j \\ \langle \mathbf{f}_k, \mathbf{f}_{i_n^j} \rangle . c_n^j + \langle \mathbf{f}_k, \mathbf{w}_j \mathbf{v}_n \rangle & \text{for } k \neq i_n^j, \end{cases} \end{aligned} \tag{11}$$

where $\mathbf{v}_n$ are the L samples around the n^{th} symbol.

The detection of the filter index $\hat{i}^j$ at the j^{th} TA is estimated according to (10) by choosing the maximum $U_k = \|r_k^j\|^2$ which represents the energy of r_k^j . Note that U_k follows the independent non-central Chi-Square distribution [24] for all k with degree of freedom equal 2 and the non-central parameter α^2 that can be expressed as follows:

$$\alpha_{k,q}^2 = \begin{cases} \|c_n^j\|^2 = \mathcal{E}_q & for\ k = i_n^j \\ \langle \mathbf{f}_k, \mathbf{f}_{i_n^j} \rangle^2 . \|c_n^j\|^2 = \langle \mathbf{f}_k, \mathbf{f}_{i_n^j} \rangle^2 . \mathcal{E}_q & for\ k \neq i_n^j, \end{cases} \tag{12}$$

where $f_{i_n^j}$ is the selected filter at the j^{th} TA and $\mathcal{E}_q$ is the transmitted energy of the APM symbol c_n^j.

Therefore, the PDF of U_k can be written as follows:

$$p(u_k) = \frac{1}{2\sigma_p^2} e^{-\frac{u_k + \alpha_k^2}{2\sigma_p^2}} \mathcal{I}_0 \left(\frac{\alpha_k \sqrt{u_k}}{\sigma_p^2} \right), \tag{13}$$

where $u_k \geq 0$, σ_p^2 is the post-equalization noise variance, and $\mathcal{I}_0(\rho)$ is the zero order modified Bessel function of 1^{st} kind given by [24]:

$$\mathcal{I}_0(\rho) = \sum_{\beta=0}^{\infty} \frac{(\rho/2)^{2\beta}}{(\beta!)^2} \ \rho \geq 0. \tag{14}$$

Since the MF-based detector for all $j = 1, \ldots, N_t$ performs APM and filter index estimation in parallel for all TAs similar to SISO-FSIM detection [19], we will consider the detection on one of the TA, and the index j is omitted. Let us suppose that the filter f_1 is selected at the transmitter side for the APM symbol c_n. The detector makes a correct index decision; if the probability of u_1 is greater than all other $N-1$ u_k values for $k \neq 1$. The filters are considered orthogonal to derive the lower bound, and thus the u_k become statistically independent, then the joint probability can be factorized as a product of $N-1$ marginal probabilities of the form:

$$P(u_k < u_1 | u_1) = \int_0^{u_1} p_{u_k}(x_k) dx_k. \ k = 2, 3, ..., N. \tag{15}$$

Hence, the probability of a correct decision is given as follows [19]:

$$\begin{aligned} P_{c,\mathcal{E}_q} &= P(U_2 < U_1, U_3 < U_1, ..., U_N < U_1) \\ &= \int_0^{\infty} \left(\prod_2^N P(u_k < u_1 | u_1) \right) . p(u_1) du_1, \end{aligned} \tag{16}$$

and the probability of a filter index error can be deduced from probability of a correct decision as:

$$P_{e,\mathcal{E}_q} = 1 - P_{c,\mathcal{E}_q}. \tag{17}$$

The average probability of filter index error ought to be the weighted average filter error accross the Q possible energy levels of APM symbols, given as follows:

$$P_{e,filter} = \sum_{q=1}^{Q} P_{e,\mathcal{E}_q} . P(\mathcal{E}_q), \tag{18}$$

where $P(\mathcal{E}_q)$ is the probability of occurrence of the energy level $\mathcal{E}_q$.

The SER of M-ary QAM modulation in AWGN channel is given by [24]:

$$P_{e,QAM} = \begin{cases} 4\left(1 - \frac{1}{\sqrt{M}}\right) Q\left(\sqrt{\frac{3}{M-1} SINR}\right) & \text{k is even} \\ \quad - 4\left[\left(1 - \frac{1}{\sqrt{M}}\right) Q\left(\sqrt{\frac{3}{M-1} SINR}\right)\right]^2 & \\ \left(\frac{4IJ - 2I - 2J}{M}\right) Q\left(\sqrt{\frac{6log_2(IJ)}{(I^2 + J^2 - 2)} SINR}\right) & \text{k is odd} \\ \quad - \frac{4}{M}(1 + IJ - I - J) Q^2\left(\sqrt{\frac{6log_2(IJ)}{(I^2 + J^2 - 2)} SINR}\right), & \end{cases} \tag{19}$$

where $SINR$ is Signal-to-Interference-plus-Noise Ratio, Q is the Q-function, $k = \log_2 M$, $I = 2^{\frac{k-1}{2}}$, and $J = 2^{\frac{k+1}{2}}$.

Subsequently, the correct detection of FSIM symbols arises when both the filter and the APM symbol are correctly estimated, therefore the probability of a correct FSIM decision at a given TA is $(1 - P_{e,filter})(1 - P_{e,QAM})$ and the SER_{FSIM} is given by:

$$SER_{\text{FSIM}} = 1 - (1 - P_{e,filter})(1 - P_{e,QAM}). \tag{20}$$

Then, the SINR estimation at the j^{th} branch can be written as:

$$SINR_j = \frac{\mathbb{E}\{\hat{s}_j^2\}}{\mathbb{E}\{\mathbf{w}_j \mathbf{v}_n\}} = \frac{P}{\|\mathbf{w}_j\|^2 \sigma^2} = \frac{SNR}{\|\mathbf{w}_j\|^2}, \quad (21)$$

where P is the average power on each TA, and SNR is the average transmitted signal to noise ratio.

We defined $\omega_j = 1/\sqrt{\|\mathbf{w}_j\|^2}$, then ω_j meets general Rayleigh distribution with variance $1/2$ and degree of freedom $2(N_t - N_r + 1)$ when the channel matrix $\mathbf{H}$ follows Rayleigh distribution. In this case, the probability density function (PDF) of ω_j is the following:

$$p_\omega(\omega_j) = \frac{2}{(N_r - N_t)!} (\omega_j)^{2(N_r - N_t)+1} e^{-(\omega_j)^2}. \quad (22)$$

In the ZF algorithm, the FSIM symbol detection is implemented independently on each branch of the equalizer output corresponding to the symbol emitted from the j^{th} TA with same configuration (filter bank, APM scheme and order), and the SINR of each sub data stream follows the same distribution with the same degree of freedom. Hence, the average SER of SMX FSIM symbol with ZF and MF based detector receiver can be obtained under any fading channel as follows:

$$\begin{aligned} \text{SER}_{\text{SMX FSIM}} &= \frac{1}{N_t} \sum_{j=1}^{N_t} (\text{SER}^j_{\text{SMX FSIM}}) = \text{SER}^j_{\text{SMX FSIM}} \\ &= \int_0^\infty SER_{FSIM}(\omega_j) p_\omega(\omega_j) d\omega_j, \end{aligned} \quad (23)$$

where the PDF $p_\omega(\omega_j)$ depends on the considered channel distribution.

IV. Results and Discussions

After considering the sub-Thz aspects in the design phase of the proposed SMX-FSIM system and its theoretical performance validation, we studied in this section the proposed transceiver in MIMO sub-THz channels generated from a ray-based deterministic channel model by our BRAVE partner [23]. In addition, we evaluated the system performance of the proposed system and other sub-THz candidates with RF impairments. Finally, different sub-THz system are compared from different perspectives to deduce the most promising candidate.

A. Theoretical and simulated performance comparison of SMX-FSIM to equivalent SMX-QAM system

In this sub-section, we evaluated our proposed system SMX-FSIM using the derived theoretical performance in a Rayleigh channel, and in the next section we will consider sub-THz channel model. Several Monte Carlo simulations are performed to validate the theoretical lower bound SER performance (23) and compared to equivalent system of the same SE. Note that the theoretical SER performance of SMX-QAM with ZF equalizer is according to [25, Eq. (9)]. In addition, the SMX-FSIM system is compared at different transmission rates to its equivalent SMX-APM systems. For a fair comparison, both systems with ZF equalizer are compared with same number of receive antennas and under the same SE, which requires either the same modulation schemes with SMX-FSIM and SMX-QAM or the same number of transmit antennas. We cannot conserve the same values for both variables because SMX-QAM needs to accommodate the virtual bits conveyed in the filter IM domain by increasing one of these parameters. The simulation parameters for all configurations in this section are summarized in Table I.

TABLE I
SIMULATION PARAMETERS

Parameters	Value
N_t for SMX-8QAM, SMX 2-FSIM-QPSK	$[4, 8, 10]$
N_t for SMX-QPSK	$[6, 12, 15]$
N_r	$[8, 12, 16]$
η	10
Oversampling factor: λ	8
Filter's length: L	81
Pulse shaping filter for Conventional Transceiver	Root Raised Cosine (RRC)
Number of channel realizations	500
Total Number of symbols	5×10^6

Figures 4-6 show the SER performance for SMX-QAM and SMX-FSIM with/without perfect ISI cancellation in Rayleigh channel by transmitting 12 to 30 bits per MIMO symbol (or bit per channel use (bpcu)). In addition, the theoretical SER for both systems are compared to the Monte Carlo simulation results. The notation $N-$FSIM-APM is used to describe FSIM scheme with N filters and APM modulation schemes.

The different systems with 12 bpcu and $N_r = 8$ are: SMX-QPSK with N_t =6, SMX $2-$FSIM-QPSK and SMX 8QAM with $N_t = 4$. As we can notice that when we are using the same QAM order M for SMX-FSIM and SMX-QAM, N_t for the SMX-QAM system is larger to have the same SE. Similarly, when the same N_t is used, the modulation order is increased for SMX-QAM for same reason. The SER performance of these systems are depicted in Fig. 4, and it is clear that SMX 2-FSIM-QPSK system has 3 dB and 5.2 dB performance gain at SER$= 10^{-4}$ compared to the equivalent SMX-8QAM and SMX-QPSK systems respectively.

Similar comparisons with larger number of transmit antennas are provided to achieve higher SE. The results in Figs. 5-6 show that SMX 2-FSIM-QPSK with $N_t = 8$ (SE=24 bpcu) and $N_t = 10$ (SE=30 bpcu) achieve around 3-3.5 dB performance gain compared to SMX-8QAM with same number of transmit antennas and more than 12 dB gain compared to SMX-QPSK.

Finally, it is worth mentioning that the simulated SER for SMX-QAM matches their theoretical curves, and the simulated SER for SMX-FISM system with perfect ISI cancellation is very tight to its theoretical lower bound in all configurations. Whereas, a slight performance degradation (less than 0.8 dB) can occur when using the proposed ISI estimation and cancellation technique due to residual ISI from the non-Nyquist filters.

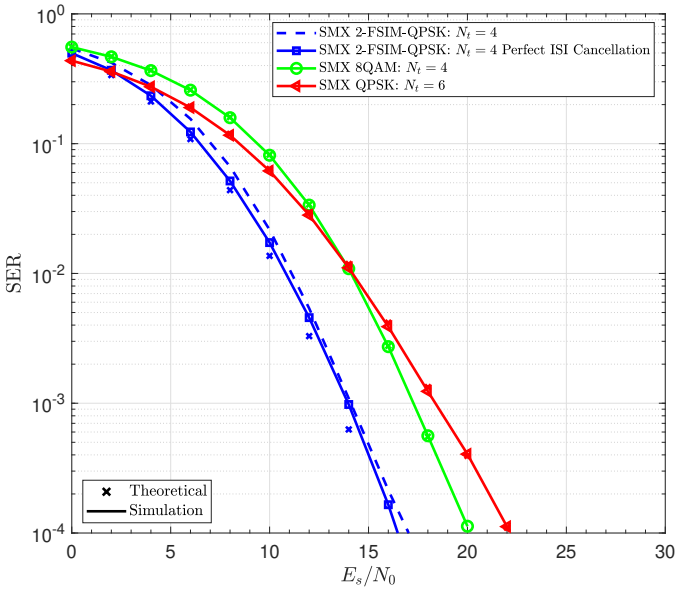

Fig. 4. SER performance of the proposed SMX 2-FSIM-QPSK system and its equivalent SMX-QAM systems of same SE= 12 bpcu and $N_r = 8$.

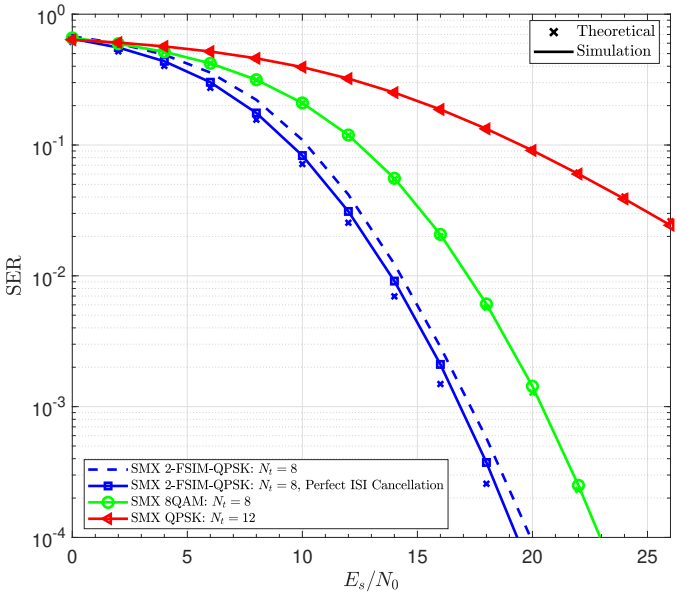

Fig. 5. SER performance of the proposed SMX 2-FSIM-QPSK system and its equivalent SMX-QAM systems of same SE= 24 bpcu and $N_r = 12$.

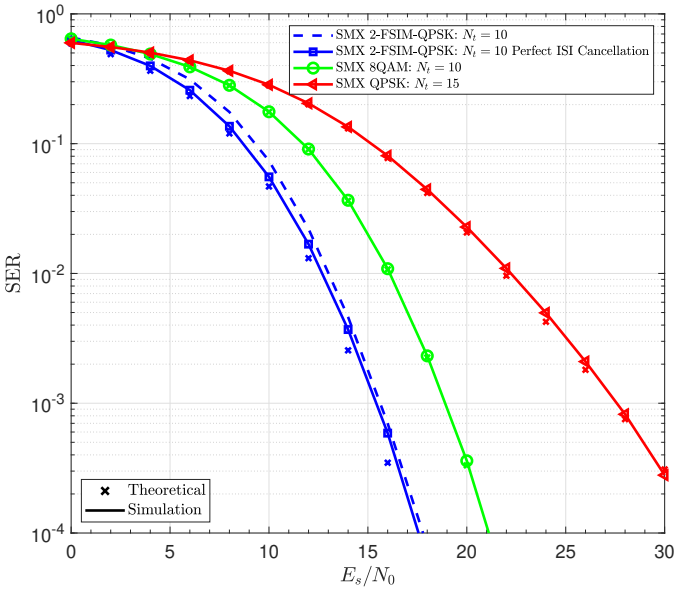

Fig. 6. SER performance of the proposed SMX 2-FSIM-QPSK system and its equivalent SMX-QAM systems of same SE= 30 bpcu and $N_r = 16$.

TABLE II
SPECTRAL EFFICIENCY OF DIFFERENT $N_t \times N_r$ MIMO TECHNIQUES.

	System Name	Spectral Efficiency $\mathcal{L}$ (bpcu)	N_a number of activated TA(s)
SMX	SMX-APM	$N_t \log_2 M$	N_t
	SMX-FSIM	$N_t \log_2 M + N_t \log_2 N$	N_t
Transmit Spatial IM	SSK [6]	$\lfloor \log_2 N_t \rfloor$	1
	GSSK [15]	$\lfloor \log_2 C_{N_t}^{N_a} \rfloor$	N_a
	Bi-SSK [26]	$2\lfloor \log_2 N_t \rfloor$	$N_a = 1$ for I/Q: $\{1, 2\}$
	ExSSK [27]	N_t	$\{0, \ldots, N_t\}$
	SM [5]	$\log_2 M + \lfloor \log_2 N_t \rfloor$	1
	GSM [7]	$N_a \log_2 M + \lfloor \log_2 C_{N_t}^{N_a} \rfloor$	N_a
	QSM [8]	$\log_2 M + 2\lfloor \log_2 N_t \rfloor$	$N_a = 1$ for I/Q: $\{1, 2\}$
	VGSM [28]	$\approx \log_2 M + \log_2(2^{N_t} - 1)$	$\{1, \ldots, N_t\}$

B. Spectral Efficiency Analysis: SMX-FSIM vs existing MIMO techniques

In this section, the spectral efficiency of different MIMO techniques with different number of TAs N_t and modulation order M is analyzed. This comparison considers the conventional SMX with linear APM (QAM, PSK), and several transmit spatial modulations with/without APM that uses the TA(s) indices to convey additional information bits. The SE of these systems are summarized in Table II while assuming $N_r \geq N_t$, and Figs 7-8 compare their SEs as function of number of TAs with $M = 4$ and $M = 16$ respectively. For clarification, the Extended SSK (ExSSK) and Variable N_a GSM (VGSM) (shown in Table II) allow a variable number of active TAs to increase the SE. For the same reason, a separate indexation for the in-phase and quadrature components is considered in Bi-SSK [26] and Quadrature SM [8].

Note that the SE of GSSK and GSM depends on the number of activated TAs N_a as shown in Table II, and in these figures N_a is selected to achieve the maximum SE with a specific N_t that occurs when $N_a = \frac{N_t}{2}$ with GSSK (depends on M-ary order with GSM using $N_a < N_t$ to enable IM since GSM using $N_a = N_t$ is same as conventional SMX). Figs. 7-8 show that the transmit spatial IM schemes without APM (i.e. SSK [6], GSSK [15], Bi-SSK [26], ExSSK [27]) suffer from a limited SE gain, and thus they are more suitable for low data rates applications. Whereas a higher SE is reached when incorporating APM symbol transmission with IM (i.e., SM, GSM, QSM, etc.). It is clear that the

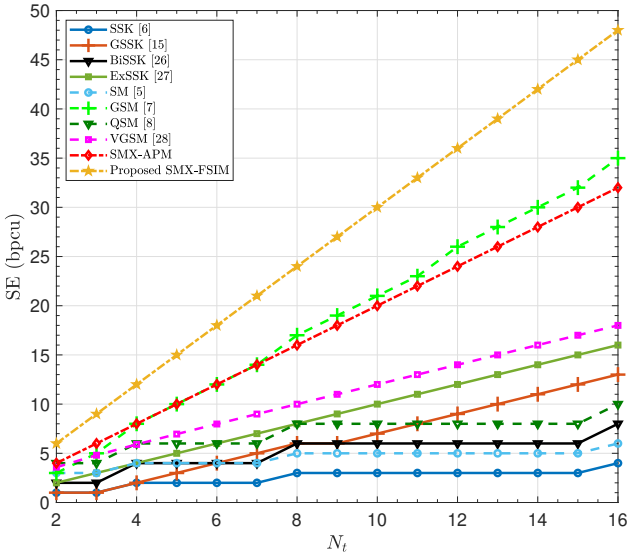

Fig. 7. Maximum SE for different MIMO techniques: $M = 4$ for systems with APM, $N_a = [1, \ldots, N_t - 1]$ for fixed N_a schemes, and $N = 2$ for FSIM.

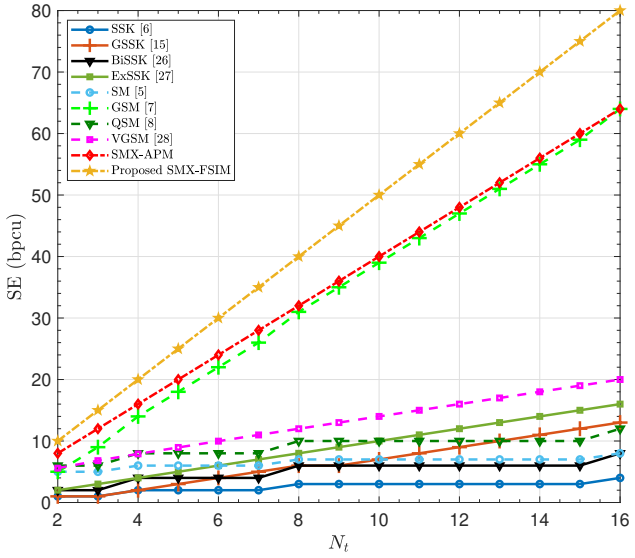

Fig. 8. Maximum SE for different MIMO techniques: $M = 16$ for systems with APM, $N_a = [1, \ldots, N_t - 1]$ for fixed N_a schemes, and $N = 2$ for FSIM.

highest SE is achieved by the conventional SMX-APM, GSM, and the proposed SMX-FSIM system due to the important multiplexing gain with/without IM. However, SMX-FSIM achieves 1.5 (resp. 1.25) times higher SE with 2 filters only compared to SMX-QPSK (resp. SMX-16QAM) as depicted in Fig. 7-8 where SMX-FSIM shows its superiority over all other MIMO techniques. In addition, it is worth mentioning that the number of activated TAs N_a with transmit spatial IM is less than N_t but they require full-RF transmit architecture (i.e. Number of RF chains = N_t) to avoid SE degradation. Note that the transmit spatial IM schemes with RF-switching having the number of RF chains equals to the maximum N_a suffer from spectral regrowth due to pulse shaping time truncation to symbol period, and thus a SE degradation will occur [29]. Moreover, the RF-switching time at each symbol period introduces additional SE degradation [30]. Thus, the obvious solution for all transmit spatial IM is to use a full-RF transmit architecture to avoid this SE problem.

C. Comparison of SMX-FSIM, conventional SMX and GSM in sub-THz environment

In this section, the best candidates in terms of SE highlighted in previous section are evaluated from different perspectives while considering sub-THz challenges and limitations. Note that SMX-QAM and GSM system are investigated in sub-THz environment in [4], [16], and the results show that using lower modulation order M is more efficient especially in sub-THz with RF impairments and limitations such as higher robustness to PN, lower transmit power and less ADC resolution requirements. For this reason, the proposed SMX-FSIM system using QPSK is compared to their equivalent GSM and SMX schemes with the same SE.

1) Performance in sub-THz channel with RF impairments: In this sub-section, these candidates' performance is evaluated under indoor sub-THz channels and subjected to PN impairment. The sub-THz MIMO channels are generated using ray-based deterministic channel model [23]. For instance, different channel realizations are generated using a ray-based deterministic channel model for sub-THz Band (mainly between 90-200 GHz) [23]. In this paper, we focused on the downlink hotspot (or kiosk) indoor scenario operating at 150 GHz where the Access Points (APs), acting as transmitters, and the User Equipments (UEs), acting as receivers, are equipped with N_t and N_r isotropic antennas respectively. The setup environment is described in [4], [23], where 10 APs mounted on the ceiling with fixed positions and 50 UEs at random positions are used to generate different channel realizations as shown in Fig. 9. In our simulations, the distance between the AP and UE is up to 8 meters (m), and its average is 5 m. The MIMO channels are obtained with Uniform-Linear-antenna Array (ULA).

For a wideband system like our case in sub-THz, the PN impairment can be modeled by Gaussian distribution with zero mean and σ_g^2 variance [21] which is the dominant term of the PN that affects the wideband system performance [22], and in the following different PN levels are considered: low $\sigma_g = 10^{-3}$, medium $\sigma_g = 10^{-2}$, and high $\sigma_g = 10^{-1}$, the used MIMO PN model is according to [4]. For a fair comparison, the SMX FSIM, SMX QAM, and GSM systems are configured to achieve the same SE of 12 bpcu with the same number of RAs, and same modulation scheme QPSK or the same number of TAs, and without PN mitigation (non-coherent detection). The configuration of these systems is summarized in Table III where we can observe the different systems of the same SE either have same M modulation order or same N_t, and they use the full-RF transmitter architecture. Note that a pulse-shaping filter is considered with all MIMO systems before transmission with the same parameters shown in Table I, and a low complexity receiver based on ZF equalizer is adopted with all systems to allow practical implementation of downlink

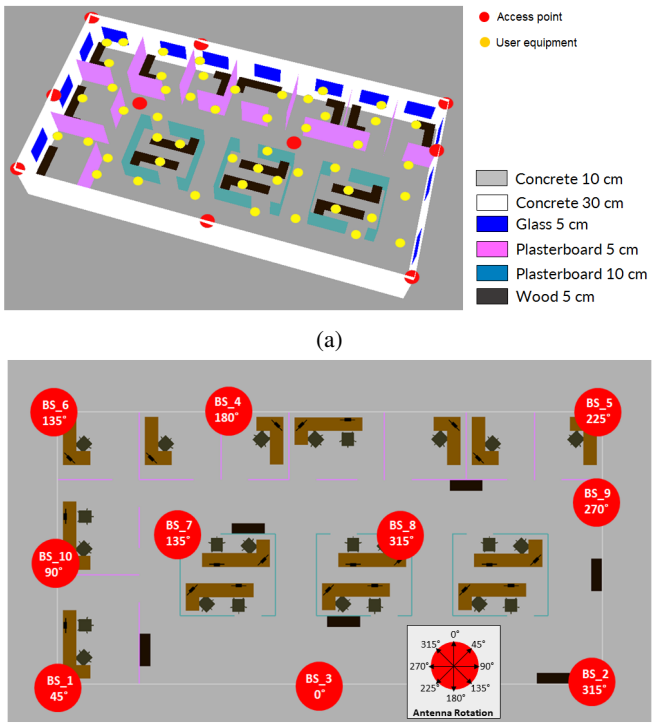

Fig. 9. Indoor MIMO channel measurements [23]. (a) 3D physical positions of 10 APs marked in red circles and 50 UEs marked in yellow. The office is composed of external walls, windows, internal walls, cubicle partitions and desks. (b) 2D positions of the 10 APs and office furniture.

scenario where the UE has complexity and energy constraints.

TABLE III
SYSTEM CONFIGURATION FOR SUB-THz CANDIDATES WITH 12 BPCU.

System	N_t	N_r	M	N_a	N
SMX-FSIM	4	10	4	4	2
SMX-QAM	4	10	8	4	1
SMX-QAM	6	10	4	6	1
GSM	6	10	4	5	1
GSM	9	10	4	3	1

The non-coherent SMX 2-FSIM-QPSK system with low and medium PN levels achieves the best performance compared to its competitor systems as depicted in Figs. 10-11. For instance, SMX 2-FSIM-QPSK has a 3.9 dB and 18 dB gain compared to SMX-8QAM with same number of TAs and SMX QPSK (same modulation) respectively. Similarly, SMX 2-FSIM-QPSK has 9.8 dB gain compared to GSM-QPSK with $N_t = 9$ and $N_a = 3$, while GSM-QPSK with $N_t = 6$ and $N_a = 5$ suffers from important error propagation that leads to error floor. The GSM system in general are more prone to error since the mis-detection of the activated TAC does not cause only virtual bit errors but it propagates to the detection of all transmitted APM symbols in the same MIMO vector due to the attempt of APM symbols detection on non-activated TAs. This drawback of GSM clearly appears when $N_t = 6$ and $N_a = 5$ in both figures, while the other GSM configuration performs better since it is well known that GSM performance is enhanced when transmitting most of the information bits by means of IM. However, the SMX FSIM system overcomes

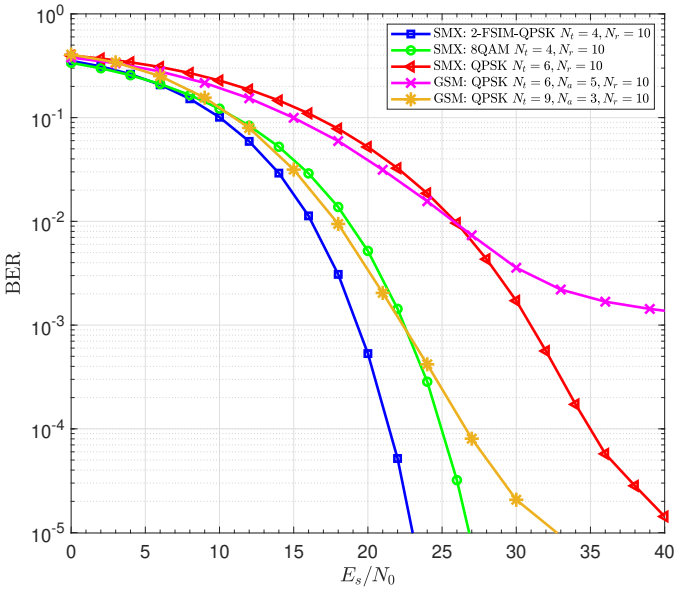

Fig. 10. Un-coded BER performance of the proposed non-coherent SMX FSIM compared to SMX-QAM and GSM in sub-THz channels with low phase noise ($\sigma_g^2 = 10^{-1}$). The SE for all systems is 12 bcpu.

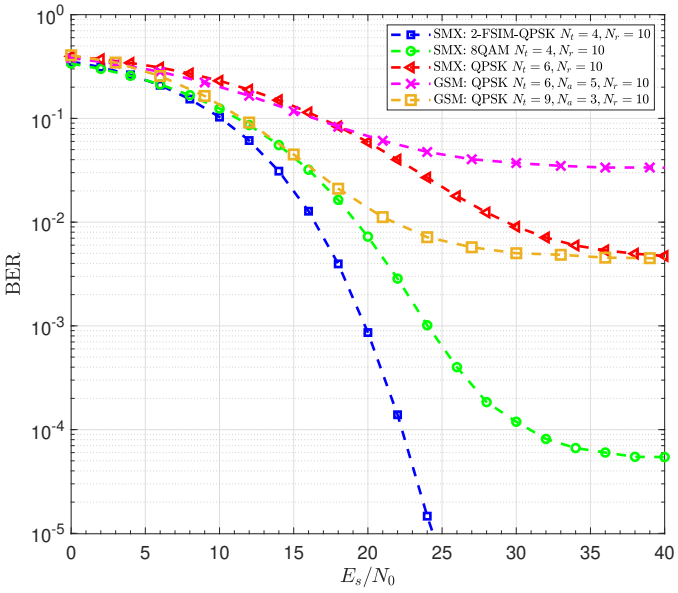

Fig. 11. Un-coded BER performance of the proposed non-coherent SMX FSIM compared to SMX-QAM and GSM in sub-THz channels with medium phase noise ($\sigma_g^2 = 10^{-2}$). The SE for all systems is 12 bcpu.

GSM drawback of error propagation to all APM symbols by the decentralization of virtual bits transmission to N_t groups of virtual bits, and thus a mis-detection of filter index can affect only the subsequent single APM symbol detection and not the all the transmitted APM symbols like in GSM. Furthermore, the filter index mis-detection does not cause necessarily an APM symbol error since the transmitted APM symbol is not completely lost in contrast to GSM that drops the APM symbols on non-activated TAs.

A similar conclusion can be drawn at medium PN level ($\sigma_g^2 = 10^{-2}$) from Fig.11. Besides, it is worth mentioning that SMX FISM with linear receiver is the only system able to

TABLE IV
AVERAGE COMPUTATIONAL COMPLEXITY IN TERMS OF REAL MULTIPLICATIONS FOR SMX-FSIM, SMX-APM, AND GSM EQUALIZERS/DETECTORS.

System	ZF equalizer/detector complexity	ML complexity
SMX-FISM	$(\frac{N_s\lambda+L-1}{N_s})4N_tN_r + N_t(\mathcal{C}_{MF} + \mathcal{C}_{\text{ISI cancellation}}) + \mathcal{C}_{W_{ZF}}/N_s$	$2^{\mathcal{L}_{\text{SMX-FSIM}}+1}(2N_t+1)LN_r$
SMX-APM	$4N_tN_r + 2MN_t + \mathcal{C}_{W_{ZF}}/N_s$	$2^{\mathcal{L}_{\text{SMX}}+1}(2N_t+1)N_r$
GSM	$4N_aN_r + 2MN_a + \mathcal{C}_{W_{ZF}}/N_s$	$2^{\mathcal{L}_{\text{GSM}}+1}(2N_a+1)N_r$

operates at this PN level without an error floor. However, all these system configurations suffer from an error floor when subjected to very high PN level ($\sigma_g^2 = 10^{-1}$). In conclusion, the non-coherent SMX FSIM provides the best PN robustness among these candidates, but a PN mitigation technique and/or an APM less sensitive to PN (e.g., PAM, spiral constellations [31], Polar QAM [32], ...) are necessary at very high PN level.

2) Complexity: In this section, we characterize these systems in terms of the computational complexity of the optimal ML and the low complexity ZF based equalizer/detector. Their average complexity per symbol is expressed in terms of Real Multiplications (RMs) and summarized in Table IV. Note that each Complex Multiplication (CM) consists of 4 RMs, and it can be computed using 3 RMs if one term in known in advance [33, Eq. (12)]. The computational complexity of the ZF matrix for the $N_r \times N_t$ channel $\mathbf{H}$ is expressed in terms of RMs as follows:

$$\mathcal{C}_{W_{ZF}} = 4(\frac{2N_t^3 + 3N_t^2 - 5N_t}{6} + 2N_rN_t^2), \tag{24}$$

where the first term is for the square matrix $\mathbf{H}^H\mathbf{H}$ inversion and the second term represents the needed multiplications to deduce the pseudo inverse of $\mathbf{H}$. However, the ZF matrix calculation can be computed once when the channel is static for the duration of N_s symbols. Note that the ZF equalization for SMX-APM and GSM can be performed after matched filtering and down-sampling, while that for SMX-FSIM should be done for the whole received signal (all samples: $N_s\lambda + L - 1$) prior to the filter index detection, and then perform the matched filtering using the detected filter. Hence, the sample level equalization for FSIM is approximately λ times larger than that of symbol level equalization.

The complexity of SMX-FSIM receiver lies in the equalization, ISI estimation and cancellation block, and the matched filter detector. The matched filter on each TA performs N convolutions with a filter of length L known in advance, then the middle sample is used for detection after sampling. Thus, this middle sample is computed by L CMs when the signals of the convolution are completely overlapped. For the filter index and APM symbol detection, $N+M$ Euclidean Distances (EDs) are computed where ED consists of 2 RMs. Thus, the matched filter complexity is expressed as:

$$\mathcal{C}_{MF} = 3NL + 2N + 2M \tag{25}$$

The ISI estimation and cancellation block (depicted in [19, Fig. 3] contains a MF detector for tentative decisions, and the Tx filter output regeneration that multiplies the estimated tentative APM symbol with the filter (L CMs$= 3L$ RMs). Similarly, the feedback of the previously detected symbol contains L CMs$= 3L$ RMs. Afterward, an overlap and add is performed to deduce the estimated ISI, then it is subtracted from the input signal where these steps contain only additions/subtractions. Therefore, the total complexity of the ISI estimation and cancellation block is:

$$\mathcal{C}_{\text{ISI cancellation}} = \mathcal{C}_{MF} + 6L. \tag{26}$$

The ZF based equalizer/detector provides a prominent complexity reduction for all systems compared to the ML counterpart, and SMX-FSIM suffers from higher receiver complexity which is proportional to the filter length L as shown in Table IV. However, it is clear from the results in Sections IV-A and IV-C1 that the performance of SMX-QAM and GSM with their linear detection are not satisfactory as SMX-FSIM and the formers have a high error floor with medium PN level ($\sigma_g = 10^{-2}$). Therefore, the additional complexity of SMX-FSIM linear receiver, compared to SMX-APM and GSM, comes with a tremendous system performance and robustness to PN that are critical factor for sub-THz system with RF impairments and limited SNR.

It is worth mentioning that the SMX-FSIM transmitter has a low complexity because the filtering operation for each symbol is a merely simple multiplication and the OLA block is composed of adders only that means FSIM transmitter does not introduce an additional noticeable computational complexity compared to other systems.

3) Hardware cost and design issues: The hardware cost depends on the number of used RF-chains that contains the most expensive hardware components. In Section IV-B, it is highlighted that the full-RF transmit architecture is required with transmit spatial IM schemes to avoid SE degradation. Therefore, the number of RF-chains at Tx side is same as number of TAs N_t with all schemes, and thus it is clear from Table III and Figs. 7-8 using any M-ary modulation scheme that SMX-FSIM system with only 2 filter shapes requires the minimum number of TAs N_t (and thus RF-chains) to achieve any SE. Therefore, SMX-FSIM allows to have the minimum possible cost for the transceiver hardware. Note that GSM receiver with some configurations can have lower cost by using smaller number of RF-chains equal to N_a, but this condition ($N_r = N_a < N_t$) can highly degrades the system performance with low complexity detectors.

It is worth mentioning that the full-RF transmitter architecture with GSM eliminates the high-speed RF switching challenge at the price of higher cost. The practical implementation of these MIMO schemes requires careful antenna array design to have low spatial correlation, and especially for GSM system since the mis-detection of the activated Transmit Antenna Combination (TAC) leads also to APM symbols error and thus highly degrades GSM overall performance [34].

TABLE V
LINK BUDGET AND POWER CONSUMPTION OF SMX FSIM, SMX QAM AND GSM SYSTEMS WITH ZF BASED DETECTION OVER SUB-THz CHANNELS SUBJECTED TO LOW PN.

System Parameters	**SMX FSIM**	**SMX 8QAM**	**SMX QPSK**	**GSM** ($N_t = 9$, $N_a = 3$)
Carrier frequency (GHz)	150.00			
Distance (m)	2 to 8			
Channel Bandwidth W (GHz)	0.50			
Required Transmit Power P_t (dBm)	0.04 to 12.09	3.94 to 15.99	18.04 to **30.09**	9.84 to **21.89**
Transmit antenna gain G_t (dBi)	20.00			
EIRP (dB)	20.04 to 32.09	23.94 to 35.99	38.04 to **50.09**	29.84 to **41.89**
$fspl$ (dB)	81.98 to 94.03			
Receive antenna gain G_r (dBi)	5.00			
Received power Rx_{level} (dBm)	-56.94	-53.04	-38.94	-47.14
Thermal noise (PSD) (dBm/Hz)	-174.00			
Noise figure N_{Figure} (dBm)	7.00			
Thermal noise $N_{Thermal}$ (dBm)	-86.94			
Noise floor N_{floor}	-79.94			
Required SNR with low PN (dB)	23.00	26.90	41.00	32.80
PAPR (dB) at CCDF= 10^{-4}	7.3	5.8	3.65	8.3
PA efficiency	0.34	0.4	0.52	0.31
Power consumption (dBm)	**4.71 to 16.75**	**7.92 to 19.96**	**20.87 to 32.92**	**14.93 to 26.97**

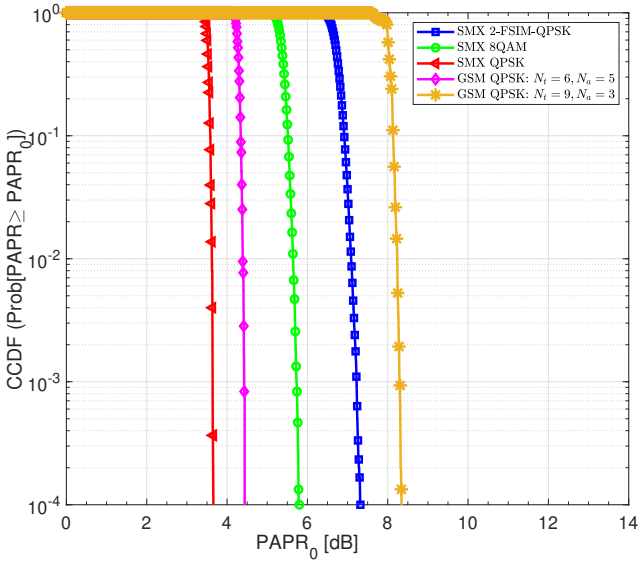

Fig. 12. Comparison of CCDF of PAPR for the SMX FSIM, the SMX QAM and the GSM systems with pulse shaping having SE= 12 bpcu. SMX FSIM uses the filter shapes presented in [19], while SMX QAM and GSM use RRC filter.

4) PAPR, Link Budget and Power consumption: Based on a MIMO SC transceiver with pulse shaping, the corresponding Complementary Cumulative Distribution Functions (CCDFs) of the PAPR of SMX-FSIM, SMX-QAM and GSM systems are shown in Fig. 12. The PAPR for all these schemes is evaluated over one TA, since all TAs for each system have similar PAPR when using same M-ary scheme for different TAs and TAs activation is equiprobable in GSM. SMX-FSIM use the non-Nyquist filter shapes designed for filter IM domain [19], while the pulse shaping for SMX-QAM and GSM system is performed with root raised cosine filter. The CCDF that represents the probability of having a PAPR higher than a $PAPR_0$ threshold depicted in Fig. 12 shows clearly that SMX QPSK have the lowest PAPR 3.65 dB at CCDF of 10^{-4}, and the PAPR increases to 5.8 dB SMX 8QAM due to the higher M-ary scheme (8QAM), and to 4.4 dB (resp. 8.3 dB) with GSM using $N_t = 6$, $N_a = 5$ (resp. $N_t = 9$, $N_a = 3$). It is clear that the PAPR of GSM increases when the ratio $\frac{N_a}{N_t}$ decreases due to the lower average power caused by zero symbol transmission when the TA is inactive. Concerning SMX-FSIM, its PAPR is 7.3 dB due to the used filter shapes that are designed to have low filter's correlation and limited ISI without any PAPR constraint. The higher PAPR reduces the Power Amplifier (PA) efficiency, and thus it affects the system power consumption. In the following, the link budget for these systems is calculated from the required SNR to achieve BER= 10^{-5} according to the following parameters:

$$
\begin{array}{lll}
N_{Thermal} & = 10\log_{10}(k.T.W) + 30 & \text{dBm} \\
N_{Floor} & = N_{Figure} + N_{Thermal} & \text{dBm} \\
Rx_{Level} & = SNR + N_{Floor} & \text{dBm} \\
fspl & = 20\log_{10}(\frac{4\pi df_c}{c}) & \text{dB} \\
EIRP & = fspl - G_r + Rx_{Level} & \text{dBm} \\
P_t & = EIRP - G_t & \text{dBm}
\end{array}
$$

where k, T, W, N_{Figure}, $fspl$, f_c, c, G_r/G_t and $EIRP$ are Boltzmann constant, the temperature in kelvin, the channel bandwidth, the noise figure, the free space path loss, the carrier frequency, the speed of light in vacuum $(c = 3 \times 10^8 m/s)$, receive/transmit antenna gain, and the effective isotropic radiated power respectively.

Furthermore, the power consumption of these systems is deduced based on the PA efficiency that depends on their PAPR.

The link budget for the different systems in indoor scenarios (Kiosk, enhanced throughput WLAN, etc.) with a distance up to 8 m is depicted in Table V, where the GSM system with $N_t = 6$, $N_a = 5$ is omitted due to the high error floor. It is clear that SMX FSIM requires the lowest transmit power to guarantee BER= 10^{-5} due to better system performance. This low transmit power requirement is an important advantage for sub-THz bands, since the output transmit power is very limited at high frequencies with current technology. The required transmit power and the EIRP make SMX QPSK and GSM with linear ZF based detector impractical in current technology while respecting EIRP regulations in contrast to their results with ML detection discussed in [4].

TABLE VI
SUMMARY OF DIFFERENT MIMO TECHNIQUES FOR LOW-POWER WIRELESS ULTRA-HIGH DATA RATES SYSTEMS IN SUB-THZ BANDS.

	MIMO systems with power-efficient low order APMs and linear based receivers		
Parameter	**SMX-FSIM**	**SMX-QAM**	**GSM** using full-RF Tx architecture
Spectral Efficiency (see Figs. 7-8)	$N_t(\log_2 M + \log_2 N)$ **High**	$N_t \log_2 M$ **Medium**	$N_a \log_2 M + \log_2 C_{N_t}^{N_a}$ where $N_a \leq N_t$ **Medium**
Robustness to PN (see Figs. 10-11)	**High**	**Low** to **Medium**	**Low** (**High** with ML[4])
PAPR (see Fig 12)	**Medium**	**Low**	**Low** to **High** (depend on M, N_a and N_t)
Energy Efficiency (see Table V)	**High**	**Medium**	**Medium**
Linear Detector Complexity (see Table IV)	**Medium** to **High** (depend on filter length)	**Medium**	**Low**
Cost based on number of RF chains (see sub-Section IV-C-3)	**Low**	**Low** to **Medium**	**High**
Flexibility (Reconfigurable System)	**High**	**Low**	**High**

In addition, it is worth mentioning that SMX-FSIM maintains its superiority in the power consumption despite the PAPR increase by the used filters due to the important performance SNR gain. For instance, SMX-FSIM with linear receiver provides a 3.21 dBm power gain compared to SMX 8QAM and more than 10 dBm compared to GSM and SMX QPSK as shown in Table V. It is worth mentioning that acquiring a wider total bandwidth in sub-THz bands by channel aggregation/bonding, adopting a higher number of filter shapes, and/or a large scale MIMO with SMX-FSIM allows achieving a low-power wireless Tbps system.

Therefore, SMX-FSIM requires less SNR to reach the desired performance even without channel coding, and the proposed system requires the minimum number of transmit antennas to achieve any SE, as shown in Figs. 7-8 that limit the transceiver cost and power consumption related to RF chains and to achieve the desired performance so a higher EE is provided. Hence, SMX-FSIM requires less parallel modulator and RF chains than the most spectral-efficient existing MIMO systems, which means lower hardware cost and power consumption even with PN impairment, as shown in Table V. This cost and power consumption of SMX-FSIM remains the minimum compared to the other candidates, even when considering a massive MIMO system exploiting beamforming gain to compensate the sub-THz/THz losses.

Note that when considering a higher PN level, all systems with linear ZF based detector suffer from an error floor except SMX-FSIM as shown Fig. 11, and the latter consumes only 1.5 dB more than its power consumption at the low PN level.

D. Summary of sub-THz candidate system

In this sub-section, a discussion summary is provided. The proposed SMX-FSIM system is shown to achieve the highest SE gain among the existing MIMO systems with/without IM even with 2 filter shapes and low order modulation. For instance, the achieved gain with SMX FSIM system is $N_t \log_2 N$ higher than that of SMX QAM using the same modulation order and the number of antennas. It is also important to mention that SMX FSIM fully utilizes all time, frequency, and spatial resources in contrast to spatial IM (e.g., GSM,...) that activates a certain number of antennas and requires a full-RF transmitter architecture. In the current study, we are focusing on an ultra-high data rates system for indoor scenarios with power and complexity constraints for the UE receiver, like downlink kiosk application and enhanced throughput WLAN. For this reason, we developed and theoretically assessed the proposed SMX FSIM system with a linear receiver based on ZF equalizer and parallel MF detectors that allow us to maintain a low and feasible receiver complexity. The performance of SMX-FSIM is very tight to the derived theoretical lower bound. Compared to the equivalent SMX QAM system of the same SE using either the same modulation order or the same number of TAs, the results reveal that SMX FSIM with a linear receiver and only two non-optimal filter shapes outperforms by 3.5 dB up to more than 12 dB these equivalent systems in Rayleigh channel. In order to complete our study and propose a new ultra-high data rate system in the sub-THz environment, a complete analysis in the sub-THz indoor environment with RF impairments is provided for the proposed system SMX FSIM, and the other candidates (SMX QAM and GSM). Finally, we showed that SMX FSIM with a linear receiver has better performance and robustness to phase noise, lower transceiver cost, higher SE/EE gain, and lower power consumption compared to its competitor candidates. Therefore, this analysis and discussion summarized in Table VI promotes SMX-FSIM with a linear receiver as a very competitive candidate for low-power wireless ultra-high data rates system in sub-THz bands.

V. CONCLUSION

In this paper, a generalized MIMO Spatial Multiplexing system is proposed, thanks to filter IM domain that generalizes many existing modulation and time/frequency IM domains. In particular, FSIM scheme is considered in the proposed system to achieve the highest SE gain ($N_t \log_2 N$) among the existing

MIMO systems by conveying the additional bits in the index of the used filter shape at each TA. The received signal of SMX FSIM suffers from IAI and ISI that are compensated using ZF equalizer and ISI estimation and cancellation block respectively. A linear receiver based on ZF equalizer and MF-based detector is proposed to avoid the high complexity of joint ML detector by performing parallel detection for all transmitted symbols. Note that the equalization is performed at sample level before matched filter and down-sampling, since the selected filter in FSIM symbol is still unknown for the receiver at this stage. In addition, the theoretical tight lower bound of the proposed SMX FSIM system is derived and verified by Monte Carlo simulations. The proposed SMX 2-FSIM-QPSK achieves at least $3-4$ dB gain compared to SMX 8QAM of the same SE and number of TAs, and the performance gain increases to more than 12 dB compared to SMX QPSK of the same SE and APM order. Furthermore, the different candidates for ultra-high data rates in sub-THz bands (SMX FSIM, SMX QAM, and GSM with linear receiver) are evaluated in sub-THz channels with RF impairments and a complete analysis/comparison is provided. The results reveals that SMX FSIM has better performance, higher robustness to PN, lower transceiver cost, higher SE/EE gain and less power consumption. However, these advantages comes with a slight receiver complexity increase which is in order of L times higher than other candidates, and this complexity can be reduced by proper design of filter bank with shorter filter length L while respecting FSIM scheme filter requirements. Finally, it is worth mentioning that SMX FSIM in sub-THz channel requires much lower SNR ($4-18$ dB less than other candidates) which is crucial for sub-THz systems with limited output power, and it is the only scheme among these candidates that can operates in a medium PN level with linear low complexity receiver.

It is worth mentioning that massive MIMO with beamforming can be exploited with SMX-FSIM by replacing each TA in the proposed transceiver with a set of TAs to better combat the high sub-THz/THz propagation losses, and this extension will be considered in our future research work. Also, we will propose more advanced receiver design and novel schemes in our proposed IM domain.

ACKNOWLEDGMENT

The research leading to these results is partially funded from the French National Research Agency (ANR-17-CE25-0013) within the frame of the project BRAVE. We would like to thank BRAVE project partner Siradel and CEA-Leti for providing the sub-THz MIMO channels from their ray-based channel simulation and PN model respectively.

REFERENCES

[1] A. Ghosh, T. A. Thomas, M. C. Cudak, R. Ratasuk, P. Moorut, F. W. Vook, T. S. Rappaport, G. R. MacCartney, S. Sun, and S. Nie, "Millimeter-wave enhanced local area systems: a high-data-rate approach for future wireless networks," *IEEE Journal on Selected Areas in Communications*, vol. 32, no. 6, pp. 1152–1163, Jun. 2014.

[2] Y. Corre, G. Gougeon, J.-B. Doré, S. Bicaïs, B. Miscopein, E. Faussurier, M. Saad, J. Palicot, and F. Bader, "Sub-THz spectrum as enabler for 6G wireless communications up to 1 Tbit/s," in *6G Wireless Summit*, Levi Lapland, Finland, Mar. 2019.

[3] French funded project-ANR-17-CE25-0013, "Back to single-carrier for beyond-5G communications above 90 GHz-(BRAVE)." [Online]. Available: http://www.brave-beyond5g.com/

[4] M. Saad, A. C. Al Ghouwayel, H. Hijazi, F. Bader, and J. Palicot, "MIMO techniques for wireless Terabits systems under sub-THz channel with RF impairments," in *2020 IEEE International Conference on Communications Workshops*, Dublin, Ireland, Jun. 2020, pp. 1–6.

[5] R. Y. Mesleh, H. Haas, S. Sinanovic, C. W. Ahn, and S. Yun, "Spatial modulation," *IEEE Transactions on Vehicular Technology*, vol. 57, no. 4, pp. 2228–2241, Jul. 2008.

[6] J. Jeganathan, A. Ghrayeb, L. Szczecinski, and A. Ceron, "Space shift keying modulation for MIMO channels," *IEEE Transactions on Wireless Communications*, vol. 8, no. 7, pp. 3692–3703, Jul. 2009.

[7] J. T. Wang, S. Y. Jia, and J. Song, "Generalised spatial modulation system with multiple active transmit antennas and low complexity detection scheme," *IEEE Transactions on Wireless Communications*, vol. 11, no. 4, pp. 1605–1615, Apr. 2012.

[8] R. Mesleh, S. S. Ikki, and H. M. Aggoune, "Quadrature spatial modulation," *IEEE Transactions on Vehicular Technology*, vol. 64, no. 6, pp. 2738–2742, Jun. 2015.

[9] L. He, J. Wang, and J. Song, "Extended spatial modulation scheme with low complexity detection algorithms," in *2014 International Wireless Communications and Mobile Computing Conference (IWCMC)*, Nicosia, Cyprus, Aug. 2014, pp. 582–587.

[10] M. Nakao, T. Ishihara, and S. Sugiura, "Single-carrier frequency domain equalization with index modulation," *IEEE Communications Letters*, vol. 21, no. 2, pp. 298–301, Feb. 2017.

[11] T. Ishihara and S. Sugiura, "Faster-than-nyquist signaling with index modulation," *IEEE Wireless Communications Letters*, vol. 6, no. 5, pp. 630–633, Oct. 2017.

[12] D. Tsonev, S. Sinanovic, and H. Haas, "Enhanced subcarrier index modulation (SIM) OFDM," in *2011 IEEE GLOBECOM Workshops (GC Wkshps)*, Houston, TX, USA, Dec. 2011, pp. 728–732.

[13] E. Basar, U. Aygolu, E. Panayirci, and H. V. Poor, "Orthogonal frequency division multiplexing with index modulation," *IEEE Transactions on Signal Processing*, vol. 61, no. 22, pp. 5536–5549, Nov. 2013.

[14] R. Fan, Y. J. Yu, and Y. L. Guan, "Generalization of orthogonal frequency division multiplexing with index modulation," *IEEE Transactions on Wireless Communications*, vol. 14, no. 10, pp. 5350–5359, Oct. 2015.

[15] J. Jeganathan, A. Ghrayeb, and L. Szczecinski, "Generalized space shift keying modulation for MIMO channels," in *2008 IEEE 19th International Symposium on Personal, Indoor and Mobile Radio Communications*, Cannes, France, Sep. 2008, pp. 1–5.

[16] M. Saad, F. Bader, A. C. Al Ghouwayel, H. Hijazi, N. Bouhel, and J. Palicot, "Generalized spatial modulation for wireless Terabits systems under sub-THz channel with RF impairments," in *ICASSP 2020 - 2020 IEEE International Conference on Acoustics, Speech and Signal Processing (ICASSP)*, Barcelona, Spain, May 2020, pp. 5135–5139.

[17] M. Saad, F. C. Lteif, A. C. Al Ghouwayel, H. Hijazi, J. Palicot, and F. Bader, "Generalized spatial modulation in highly correlated channels," in *2019 IEEE 30th International Symposium on Personal, Indoor and Mobile Radio Communications (PIMRC Workshops)*, Istanbul,Turkey, Sep. 2019, pp. 1–6.

[18] M. Nakao and S. Sugiura, "Spectrally efficient frequency division multiplexing with index-modulated non-orthogonal subcarriers," *IEEE Wireless Communications Letters*, vol. 8, no. 1, pp. 233–236, Feb. 2019.

[19] M. Saad, J. Palicot, F. Bader, A. C. Al Ghouwayel, and H. Hijazi, "A Novel Index Modulation Dimension based on Filter Domain: Filter Shapes Index Modulation," *IEEE Transactions on Communications*, Nov. 2020, doi: 10.1109/TCOMM.2020.3039842.

[20] E. Basar, "Multiple-input multiple-output OFDM with index modulation," *IEEE Signal Processing Letters*, vol. 22, no. 12, pp. 2259–2263, Dec. 2015.

[21] S. Bicais and J.-B. Doré, "Phase noise model selection for sub-THz communications," in *2019 IEEE Global Communications Conference (GLOBECOM)*, Waikoloa, HI, USA, Dec. 2019, pp. 1–6.

[22] M. R. Khanzadi, D. Kuylenstierna, A. Panahi, T. Eriksson, and H. Zirath, "Calculation of the performance of communication systems from measured oscillator phase noise," *IEEE Transactions on Circuits and Systems I: Regular Papers*, vol. 61, no. 5, pp. 1553–1565, May 2014.

[23] G. Gougeon, Y. Corre, and M. Z. Aslam, "Ray-based deterministic channel modelling for sub-THz band," in *2019 IEEE 30th International Symposium on Personal, Indoor and Mobile Radio Communications (PIMRC Workshops)*, Istanbul, Turkey, Sep. 2019, pp. 1–6.

[24] J. Proakis and M. Salehi, *Digital communications*. Boston, MA: McGraw-Hill, 2008.

[25] J. Xu, X. Tao, and P. Zhang, "Analytical SER performance bound of M-QAM MIMO system with ZF-SIC receiver," in *2008 IEEE International Conference on Communications*, Beijing, China, 2008, pp. 5103–5107.
[26] H.-W. Liang, R. Y. Chang, W.-H. Chung, H. Zhang, and S.-Y. Kuo, "Bi-space shift keying modulation for MIMO systems," *IEEE Communications Letters*, vol. 16, no. 8, pp. 1161–1164, Aug. 2012.
[27] A. Mokh, M. Helard, and M. Crussiere, "Space Shift Keying Modulations for Low Complexity Internet-of-Things Devices," in *GLOBECOM 2017 - 2017 IEEE Global Communications Conference*, Singapore, Dec. 2017, pp. 1–7.
[28] P. Liu, M. Di Renzo, and A. Springer, "Variable- N_u generalized spatial modulation for indoor LOS mmWave communication: Performance optimization and novel switching structure," *IEEE Transactions on Communications*, vol. 65, no. 6, pp. 2625–2640, Jun. 2017.
[29] K. Ishibashi and S. Sugiura, "Effects of antenna switching on band-limited spatial modulation," *IEEE Wireless Communications Letters*, vol. 3, no. 4, pp. 345–348, Aug. 2014.
[30] E. Soujeri and G. Kaddoum, "The impact of antenna switching time on spatial modulation," *IEEE Wireless Communications Letters*, vol. 5, no. 3, pp. 256–259, Jun. 2016.
[31] A. Ugolini, A. Piemontese, and T. Eriksson, "Spiral constellations for phase noise channels," *IEEE Transactions on Communications*, vol. 67, no. 11, pp. 7799–7810, 2019.
[32] S. Bicais and J. Doré, "Design of digital communications for strong phase noise channels," *IEEE Open Journal of Vehicular Technology*, vol. 1, pp. 227–243, 2020.
[33] M. Saad, A. Al-Ghouwayel, and H. Hijazi, "UFMC transceiver complexity reduction," in *2018 25th International Conference on Telecommunications (ICT)*, St. Malo, France, Jun. 2018, pp. 295–301.
[34] M. Saad, F. Bader, J. Palicot, A. C. Al Ghouwayel, and H. Hijazi, "Single carrier with index modulation for low power terabit systems," in *2019 IEEE Wireless Communications and Networking Conference (WCNC)*, Marrakech, Morocco, Apr. 2019, pp. 1–7.

Majed Saad received the M. Sc degree with the highest distinction in computer and communication engineering (CCE) in 2016 from Lebanese International University (LIU), Beirut, Lebanon. He secured the first rank during his M.Sc. studies in the CCE Department on all LIU campuses, Lebanon. He received his PhD in Signal Processing and Telecommunications in 2020 from CentraleSupélec, Rennes, France. From October 2016 to February 2020, he was also a Lab Instructor at the school of engineering of LIU. Since January 2018, he is involved in the BRAVE French national project (ANR) about Beyond 5G Terabits wireless communication in the sub-TeraHertz bands. From September 2020, he is working as a Post-Doctoral researcher at CentraleSupélec, France. His general research interests include beyond 5G, millimeter, sub-THz and Terahertz systems, MIMO systems, Index Modulation, signal processing, and equalization. He received a grant from CNRS GdR-ISIS in France for mobility and cooperation with the University of Patras, Greece, in 2019. He also served as a Reviewer for several IEEE conferences and IEEE Transactions on Communications.

Nour Mohammad Ali Al Akkad recieved the M.Sc. degree with the highest distinction in computer and communication engineering in 2020 from the Lebanese International University, Saida, Lebanon. During her M.Sc studies, she secured the first rank in the CCE department on all LIU campuses, Lebanon. Her general research interests includes beyond 5G, sub-THz and terahertz systems, MIMO systems, index modulation, signal processing, and equalization.

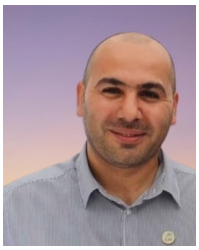

Hussein Hijazi received his B.E. degree in Computer and Communications Engineering in 2004 from the Lebanese University, Beirut, Lebanon, his M.S. degree and Ph.D. in Signal Processing and Communications in 2005 and 2008 respectively from Polytechnic Institute of Grenoble (Grenoble-INP), Grenoble, France. Dr. Hijazi earned a Ph.D. Award 2010 at Polytechnic Institute of Grenoble, Grenoble, France. From September 2008 to August 2009, he was an assistant professor at the schools of engineering ENSIMAG, PHELMA and ENSE3 of Grenoble-INP. From September 2009 to December 2009, he was a Research engineer in telecommunications at National Center for Scientific Research (CNRS) - University of Lille 1, TELICE Laboratory. From December 2009 to December 2010, he was a Post-doctoral researcher at France Telecom-orange Labs, RD center, Meylan, France. Since 2010, he has joined the computer and communications engineering department at Lebanese International University (LIU) where he is currently an Associate Professor. His general research interests lie in the areas of signal processing and communications, including synchronization, time-varying channel estimation and equalization algorithms for wireless digital communications, multi-carrier and MIMO systems, modulation index, beyond-5G communications above 90GHz (Terabit systems) and IoT technologies: detection and synchronization.

Ali Chamas Al Ghouwayel received his B.E. degree in Physics-Electronics in 2002 from the Lebanese University, Beirut, his B.E. degree in Electronics Engineering and his M.S. Degree in Telecommunications in 2004 from the National School of Engineering of Brest (ENIB), Brest, France, and his Ph.D. in Signal Processing and Telecommunications in 2008 from the High School of Electricity (Supélec) and University of Rennes 1, Rennes, France. His research activities concerned Parametrization Study for Software Defined Radio Systems. In 2008, He joined the Lab-STICC laboratory in Lorient, France and worked as a Post-Doctoral researcher on the European Project DAVINCI. In 2010, He joined the Lebanese International University, in Beirut, Lebanon, as Assistant Professor and then promoted to the rank of Associate Professor in 2016. His research interests include Study, Algorithmic Optimization, Adequation Algorithm-Architecture, and Hardware prototyping and Implementation of ultra-throughput Forward Error Correction (FEC) decoders on FPGA and ASIC technologies. His recent research activities include the investigation of new technologies and signaling techniques enabling the usage of the spectrum in the sub-THz bands 90GHz-200GHz. He participated as principal investigator in the ANR Project (QCSP: Quasi-Cyclic Short Packet) aiming at the contribution to the design of future Internet of Things (IoT) networks by defining, implementing, and testing new coded modulation schemes dedicated to IoT networks. He has several refereed journal and conference papers. He also served as Reviewer for several IEEE Transactions Journals and TPC for IEEE Conferences. In August 2020, he joined the School of Engineering EFREI Paris as Chair of the Major Avionics and Space.

Faouzi Bader (M'02–SM'07) received the Ph.D. degree (Hons.) in telecommunications from the Universidad Politécnica de Madrid, Madrid, Spain, in 2002. He joined the Centre Technològic de Telecomunicacion de Catalunya-CTTC, Barcelona-Spain, as Research Associate in 2002, and he has been Senior Research Associate from 2006 to 2013. Since June 2013-2019, he has been Associate Professor at CentraleSupélec, France. Since 2017, he is Honorary Adjunct Professor with University Technology Sydney-UTS, Australia. Starting 2020, he is the Director of Research at the "Institut Supérieur d'Électronique de Paris"-ISEP, France. His research activities are mainly on ICT advanced systems as: THz wireless communications, 5G and beyond networks, and cognitive radio communication environments. He has been involved in several European projects from the 5th–7th EC research frameworks, and the general coordinator and manager of the EC funded ICT "EMPhAtiC" project focusing on "Enhanced Multicarrier Techniques for Professional Ad-Hoc and Cell-Based Communications". He has published over 34 journals and 132 papers in peer-reviewed international conferences, 13 book chapters, and 5 edited books.

Jacques Palicot received, in 1983, his Ph.D. degree in signal processing from the University of Rennes. He is now Emeritus Professor with CentraleSupelec, formerly Supélec. He was head of the Signal, Communications and Embedded Electronics (SCEE) research team until January 2019. His research focuses on adaptive signal processing for digital communications, automatic measurements techniques, software radio, cognitive radio, and Green Radio. He has taken an active part in various international bodies EBU, CCIR, URSI, and within RACE, ACTS and IST European projects He is author or co-author of more than 380 papers among them more than 80 internationals journals, three books and 25 patents. He served as Associate Editor for EURASIP JASP (2008-19). He also served as lead guest editor for Special Issues on Software Radio, Cognitive Radio and Green Radio. He has been General Chairman of ICT 2018, Next-GWiN 2014, ISCIT 2011. Technical Program Chairman of CROWNCOM 2009,2016 GREENCOM 2013, CRN Symposium ICC 2014. He is Fellow member of SEE since 2016 and he received the URSI-France medal in 2020.